IEEE Transactions on Nuclear Science, Vol. NS-28, No. 3, June 1981

ANTIPROTON COLLECTION FROM A PRODUCTION TARGET

Frank Krienen* and J. A. MacLachlan
Fermi National Accelerator Laboratory†
Batavia, Illinois 60510

Abstract

We review several aspects of the production and the collection of antiprotons produced by high energy beams of high intensity. The goal is to optimize in cost the number of antiprotons of given momentum bite one can accumulate per unit of time. Aspects which are dealt with entail the antiproton production spectrum, proton beam emittance, multiple scattering, antiproton acceptance, and phase-space matching, including chromaticity. Several hardware alternatives are considered.

I. Introduction

Fermilab is developing a proton-antiproton colliding beam facility based on the accumulation of an intense circulating beam of antiprotons from a production target struck by protons of about 100 GeV from the Main Ring. Both stochastic and electron cooling techniques will be employed to increase the density of the $\bar{p}$ beam in longitudinal and transverse phase space to achieve a peak luminosity $\gtrsim 10^{30}$ cm^{-2} from about 10^{11} antiprotons and 10^{12} protons in the Tevatron. The economic optimization of the average interaction rate depends not only on the cost of attaining the peak luminosity but also on the time required to collect the antiprotons. Thus, so long as the accumulation time is comparable to the lifetime of the colliding beams, the cost per interaction can be reduced almost in proportion to any gain that can be made in the rate of $\bar{p}$ production within the acceptance of the cooler-accumulator ring. Because the production angle distribution is broad and large acceptance rings are expensive, the economics favor a very small proton beam spot on the production target.

The precooler and accumulator authorized for construction in the Tevatron Phase I project[1] have been designed to be compatible with a range of possible production energies in the vicinity of 5 GeV and some combination of transverse acceptance and momentum bite around $10\pi \times 10^{-6}$ m and 1% respectively. The current choice of the parameters directly relevant to targeting requirements is given in Table I.

Table I. Targeting Parameters for Tevatron Phase I.

P	Proton momentum	80 GeV/c
p	Antiproton momentum	5.4 GeV/c
ε	Rms proton beam emittance ($\varepsilon \equiv \varepsilon_x = \varepsilon_y$)	$5\pi \times 10^{-8}$ m
$\bar{\varepsilon}$	Antiproton acceptance (aperture limit)	$5\pi \times 10^{-6}$ m
β_0	Proton beam width Twiss parameter at target waist ($\beta_0 \equiv \beta_{x0} = \beta_{y0}$)	1 m
$\bar{B}_0$	Antiproton beam width parameter at target waist ($\bar{B}_0 \equiv \bar{B}_{x0} = \bar{B}_{y0}$)	.04 m
$\Delta p/p$	Momentum bite accepted from target (full width)	1%
L	Length of tungsten target	.03 m
N	Number of protons/Main Ring cycle	2.6×10^{13}

*Visitor from CERN Laboratory, Geneva, Switzerland.
†Operated by Universitites Research Association, Inc., under contract with the U. S. Department of energy.

In the following we discuss the effects of these parameters on the number of antiprotons accepted per Main Ring cycle. We consider the acceptance and matching with parameters appropriate to collection optics and target station of the type discussed in a companion paper at this conference.[2] In this design the antiprotons diverging from the target are focussed by a lithium lens, an axially symmetric lens consisting of a high current conductor of lithium. Such a lens can be made for short focal length f ~ 0.1 m and large angular acceptance $\Delta\theta \sim \pm 0.05$ rad. The results in this paper show why such a device is favored for the acceptance and momentum bite desired.

II. General Formulation

Conceptually, the antiproton production $\bar{N}$ is the product of four factors: a beam factor characterized by the number of protons and the spot size, a production factor containing the cross section per nucleon and the momentum distribution of the products, a target factor determined by the length of the target and the target material, and a collection efficiency containing the transverse and momentum acceptances. For each element ds of a target of length L one can write the production in a form which nearly achieves such a factorization:

$$d^5\bar{N} = \frac{1}{\sigma_{abs}} \left(E \frac{d^3\sigma}{dp^3}\right)_{p_\perp=0} u(p_\parallel) e^{-p_\perp^2/2\,\bar{p}_\perp^2} e^{-s/\lambda} e^{-(L-s)/\bar{\lambda}} \cdot v(r,s)\, \varepsilon(r,p_\perp,\Delta p_\parallel,s)\, r\,dr\, \frac{dp^3}{p}\, \frac{ds}{\lambda}. \quad (1)$$

The various quantities are defined in Table II.

The collection efficiency ε is not strictly factorizable, however, so that discussion of the various factors independently for a target of finite length involves approximations. Most of these approximations are very good for the ranges of angle, momentum, and target length appropriate to the Tevatron I application, being indeed far more precise than experimental knowledge of the cross section.[3] There is already an approximation made in writing Eq. (1) by using the per nucleon cross section, viz., that the invariant cross section has the same dependence on atomic number as the inelastic cross section. Thus, the only A-dependence in Eq. (1) is implicit in the proton interaction length

$$\lambda = A/(\rho N_0 \sigma_{abs} A^{.69}). \quad (2)$$

The production is therefore proportional to the number of interacting protons regardless of target nucleus. However, neither the A-dependence nor the cross section value are well measured in the range of projectile and particle momenta of interest. Although the absolute antiproton yield calculated could be in error by as much as a factor of two, the dependence of relative yield on the various parameters is rather well known. We take for the cross section $(Ed^3\sigma/dp^3)_{p_\perp = 0} = 0.8$ mb/GeV^2.

Because we never consider $\Delta p/p$ of more than a few percent we always take $u(p_\parallel) = 1$. In Section V

0018-9499/81/0600-2711$00.75©1981 IEEE

Table II. Definition of quantities in yield formulae.

N	Number of protons on target per pulse
$\bar{N}$	The number of antiprotons produced within specified acceptance
s	Coordinate along beam direction, $s = 0$ at beginning of target
s_0	The location of the beam waist
$p_\parallel$	Longitudinal antiproton momentum
$p_\perp$	Transverse antiproton momentum
σ_{abs}	Proton inelastic cross section per nucleon
$(E\frac{d^3\sigma}{dp^3})_{p_\perp=0}$	Invariant cross section for inclusive forward production of antiprotons per nucleon for proton momentum P, 0.8 mb/GeV^2
$u(p_\parallel)$	Longitudinal momentum distribution function
$v(r,s)$	Radial distribution of protons in beam (normalized to N)
λ	Proton absorption length in target
$\bar{\lambda}$	Antiproton interaction length including elastic scattering
$\varepsilon(r,p_\perp,\Delta p_\parallel,s)$	The relative collection efficiency, $(\varepsilon(0,0,0,s_0) \equiv 1)$
$\Delta\Omega_0$	Solid angle acceptance at the target focus
ρ	Target density (g/cm^3)
A	Target material atomic number
N_0	Avagadro number, 6.022×10^{23}

we describe monte carlo calculation of the five-fold integration of Eq. (1) including in addition the effects of multiple coulomb and elastic nuclear scattering. The numerical results agree quite acceptably with analytic calculations discussed in Sections III and IV which are based on simplified yield formulae. In Section III we calculate optimum target length for specified material, proton beam size, and acceptance. In Section IV we derive an analytic formula for the transverse capture efficiency as a function of target length and acceptance matching. The effect of proton beam width is also calculated approximately. Yield is tabulated for several values of target length, acceptance, matching parameters, and $p_\perp$ distribution. In Section V results are given for monte carlo calculation of the antiproton yield including the proerpties of the lithium lens used as the first collection device.

III. Optimum Target Length

The general features of the yield formula Eq. (1) can be represented in an approximate form amenable to easier interpretation:[4]

$$\bar{N}/N = (d^2\bar{N}/dpd\Omega)\,\Delta p\Delta\Omega_0 L_{eff}/\lambda, \qquad (3)$$

where the differential production per interaction length per proton is given by the per nucleon cross section as

$$d^2\bar{N}/dpd\Omega = (1/\sigma_{abs})\; d^2\sigma/dpd\Omega \qquad (4)$$

and

$$L_{eff} = \int_0^L \frac{\beta_0\bar{\beta}_0\, e^{-s/\lambda} e^{-(L-s)/\bar{\lambda}}}{[\beta_0 + (s-s_0)^2/\beta_0]\;[\bar{\beta}_0 + (s-s_0)^2/\bar{\beta}_0]}\, ds \qquad (5)$$

is an effective target length which corrects the yield for $\bar{p}$ absorption, spreading of the proton beam, and tilt of the acceptance ellipse. No account is taken of the contribution of the $p_\perp$ distribution in this form; the treatment of the acecptance is approximate. This formulation has the virtue that it leads to a straightforward estimate of optimum target length for a given choice of material and proton beam size. That choice is dictated by what target materials can withstand. If we allow the per-pulse energy deposition to raise the target from 20°C to one half its melting temperature, we are limited to about 200 J/g in tungsten and about 1 kJ/g in beryllium. These materials are the optimum choices for dense, localized target and high intensity beam respectively. Using results of the intranuclear cascade program CASSIM[5] we find that for an rms beam radius 0.2 mm one can hope to handle 2×10^{12} protons on a tungsten target and possibly 8×10^{12} on a beryllium target during a fast spill. Because neither target can accept the entire Main-Ring beam and because we would like if anything a smaller beam spot to get a reasonable fraction of the production cone into the precooler acceptance, we are left with a complex optimization problem involving spot size, target material, and subdivision of the Main-Ring pulse with concommitant r.f. stacking or "box car loading" of the antiprotons into the precooler. The current choice for the solution to this problem is to use a tungsten target in a beam of 13 batches of 2×10^{12} protons focussed to a radius of 0.2 mm rms separated in time by 200 ms. The resulting antiproton batches are to be accepted with $\bar{\varepsilon} = 5\pi \times 10^{-6}$ m and $\Delta p/p = 1$ % for rf stacking into the precooler ring. The optimum length for this target determined by maximizing L_{eff} with respect to L and s_0 is 5.7 cm or 0.56 interaction lengths with the focus located 0.3 cm downstream of the center; the yield from Eq. (3) is $\bar{N}/N = 0.62\times10^{-6}$. An optimum beryllium target for the same beam size would be 0.38 interaction lengths to yield 0.42×10^{-6} antiprotons per proton. For this acceptance the contribution of depth of field to L_{eff} is secondary. As demonstrated in Section V, beryllium becomes more competitive with tungsten for production into small acceptance because its multiple coulomb scattering is negligible; the monte carlo gives a yield of about 0.8×10^{-6} for both cases. If one asks that the target be able to accept a full Main-Ring beam of 2.7×10^{13} protons in a 1.6μ sec spill, β_0 must be chosen large to preserve the target. Therefore depth of field becomes even less significant. For tungsten, a beam radius ~1 mm rms is required implying $\beta_0 = 20$ m. For beryllium a beam radius about 0.5 mm rms is suitable for which the β_0 is about 5 m. The $\bar{N}$ calculated from Eq. (3) is $\sim8.1\times10^5$ for the 7.5 cm tungsten target and $\sim3.1\times10^6$ for the 26 cm beryllium target. The factor of four advantage in solid angle for the beryllium target far outweighs its slight disadvantage in L_{eff}/λ in this extreme case.

IV. Analytic Calculation of Matched Acceptance

A. We consider next a simplified yield formula employed by several authors[4]

$$\bar{N}/N = \frac{d^2\bar{N}}{dpd\Omega}\,\Delta p\Delta\Omega_0 x_{abs} F_{geom}, \qquad (6)$$

which comes from Eq. (1) when the effect of the $p_\perp$ distribution is combined with the acceptance function ε and averaged over the target length to give a collection efficiency F_{geom} while the absorption terms are intergrated separately to give

$$x_{abs} = \int_0^L e^{-s/\lambda} e^{-(L-s)/\bar{\lambda}}\,\frac{ds}{\bar{\lambda}} = \begin{cases} (e^{-L/\lambda} - e^{-L/\bar{\lambda}})/(\lambda/\bar{\lambda}-1) & \lambda\neq\bar{\lambda} \\ L/\lambda\; e^{-L/\lambda} & \lambda=\bar{\lambda} \end{cases} \qquad (7)$$

The transverse acceptance factor F_{geom} expresses the efficiency of collection of the antiprotons within $\Delta\Omega_0$ arising from the matching of the acceptance to the production phase space and the variation of that matching over the length of the target.

There are two shortcomings of Eq. (6) which make F_{geom} an obscure quantity, not simply an independent transverse collection efficiency factor. First, $\Delta\Omega_0$ can not be chosen freely without regard for the acceptance of the collection system. Also, the definition of x_{abs} [Eq. (7)] does not reflect the relation between target length and collection efficiency which results in substantially higher yield for short absorbtion length. In the following we unravel F_{geom} so that antiproton yield is expressed in easily understood physical parameters.

B. Because the smaller the beam spot the larger the angle that can be accepted for fixed acceptance, the yield from a line source of the same length as the target will set an upper limit on the attainable yield. Starting from such a model we have the advantage that no obscure parameters will appear in antiproton yield. Taking $\lambda = \bar{\lambda}$ we assume first a constant line intensity I antiprotons m^{-1} sr^{-1}

$$I = N(d^2\bar{N}/dpd\Omega)\cdot\Delta p\cdot 1/\lambda\cdot e^{-L/\lambda}. \qquad (8)$$

We take the phase-space planes (x,x′) and (y,y′) at the beam focus so that the acceptances are upright, and we assume them equal. For the density in a certain point x,x′ we observe that the source point is located at $z = x/x'$ and the points in the (y,y′) plane contributing to the density in point x,x′ are given by $x/x' = y/y'$ as shown in Fig. 1. Now we trace a closed loop ABCD in the (x,x′) plane in a special way shown in Fig. 2. The area enclosed by the loop is dx dx′. We note that the points A and C

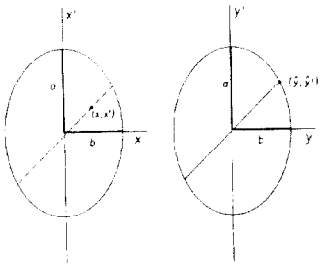

Fig. 1.

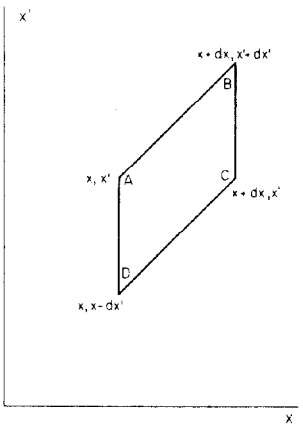

Fig. 2.

have the same ordinate. We visualize the contributions to point A in the perspective drawing (Fig. 3), where the contributing rays lie in the plane A, with a cut-off at the intersection y. Similarly, the four planes A, B, C, and D may be shown in projection on the (x,z) plane, where we note that the intersects A and C are parallel. Thus it is seen that each source point of the element dz illuminates the same area dx dx′, i.e., the soild angle dΩ will be

$$d\Omega = 2\,\hat{y}\,z^{-2}\,dx. \qquad (9)$$

From the same figure we deduce

$$dz/z = dx/x = dx'/x'. \qquad (10)$$

Because $\hat{y}$ is on the boundary of the acceptance ellipse,

$$\hat{y} = x\,(x'^2/a^2 + x^2/b^2)^{-1/2}. \qquad (11)$$

Then the flux inside the area dx dx′ will be

$$I\,dz\,d\Omega = 2\,I\,(x'^2/a^2 + x^2/b^2)^{-1/2}\,dx\,dx' \qquad (12)$$

or the density

$$D = 2\,I\,(x'^2/a^2 + x^2/b^2)^{-1/2} \qquad (13)$$

antiprotons m^{-1} rad $^{-1}$, and lines of constant density are ellipses concentric with the acceptance ellipse. On the acceptance ellipse the density is 2 I. The total number of accepted antiprotons is found by integration over the ellipse covered by the target length L. Using

$$x_0/c = x_0'/a = b\,(b^2 + c^2)^{-1/2} \text{ and } c/a = z_{max} = L/2,$$

we obtain (see Fig. 4)

$$\bar{N} = \iint D\,dx\,dx' = 8\,ab\,I\,\tan^{-1}(c/b) \qquad (14)$$

or

$$\bar{N}/N = 8(d^2\bar{N}/dpd\Omega)\cdot\Delta p\cdot 1/\lambda\cdot\exp(-L/\lambda)\,ab\,\tan^{-1}(aL/2b). \qquad (15)$$

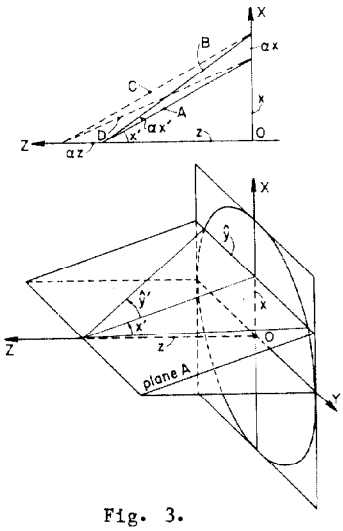

Fig. 3.

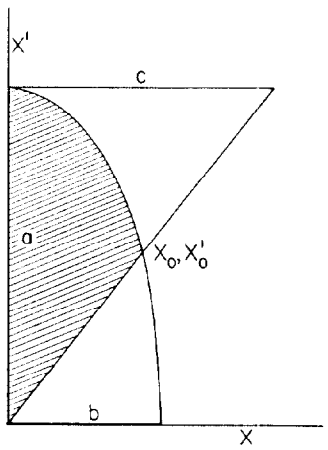

Fig. 4.

This clearly demonstrates the importance of small λ. We note that the yield equation is exact provided that the line source is on the optical axis, the production spectrum is flat over Δp and over $\theta_{max} = a$, and the multiple scattering is ignored. The equation for $\bar{N}$ contains the product $ab = \bar{\varepsilon}/\pi$. If the acceptances $\bar{\varepsilon}_x$ and $\bar{\varepsilon}_y$ are unequal, but have the same aspect ratio, we would obtain $\bar{N} = 8\,I(\bar{\varepsilon}_x\bar{\varepsilon}_y)^{1/2}\times\tan^{-1}(c/b)$, scaling with the square root of the acceptance in each plane. In the case of a short target the yield becomes $N = 4\,I\,a^2\,L$.

C. In practice one has to consider the angular dependence of the production. Fitting the simplest power series $I = I_0\,(1-m^2\theta^2)$ in which $\theta^2 = x'^2 + y'^2$ we start by observing that the elementary area $2\,\hat{y}\,dx$ is illuminated from the source element dz with a strength dependent on the emission angle. Hence,

$$I\,dz\,d\Omega = 2\,I_0 z^{-2}\,dx\,dz\int_0^{\hat{y}}[1 - m^2(x'^2 + y'^2)]\,dy, \qquad (16)$$

from which follows

$$D = 2\, I_0(x'^2/a + x^2/b)^{-1/2}[1 - m^2x'^2 + \\ - 1/3\ m^2x'^2(x'^2/a^2 + x^2/b^2)^{-1}]. \quad (17)$$

Integrating this over the area of the acceptance ellipse covered by the target length

$$\bar{N} = 8\, I_0\, ab[\tan^{-1}(c/b) - 1/3m^2a^2\{\tan^{-1}(c/b) + \\ + bc/(c^2+b^2)\}] \quad (18)$$

or

$$\bar{N}/N = 8(d^2\bar{N}/dpd\Omega)\cdot\Delta p\cdot Y, \quad (19)$$

in which the yield Y contains the natural constants λ and m^2 and the geometrical constants a, b, and L:

$$Y = 1/\lambda\ e^{-L/\lambda}ab[\tan^{-1}(La/2b) - 1/3\ m^2a^2\{\tan^{-1}(La/2b) + \\ + 1/2\ Lab/(b^2+L^2a^2/4)\}]. \quad (20)$$

This equation applies if the line source is on the optical axis, the production spectrum is flat over Δp, and multiple scattering is ignored. In Table III we give the yield Y vs. the maximum angle

Table III. Yield vs. Target Length and Acceptance Parameters.

A — $10^6 \times Y$ (m^2 = 150 rad^{-2}, λ = 0.1 m)

a mrad \ L m	b = 0.1 mm				b = 0.2 mm			
	0.06	0.03	0.01	0.005	0.06	0.03	0.02	0.01
10	6.8	7.2	4.2	2.3	11.0	9.5	7.5	4.4
20	15.0	19.0	14.0	8.5	27.0	28.0	25.0	16.0
30	23.0	28.0	25.0	17.0	42.0	48.0	45.0	32.0
40	30.0	38.0	36.0	26.0	56.0	67.0	65.0	49.0
50	36.0	46.0	44.0	34.0	68.0	83.0	82.0	65.0
60	41.0	52.0	53.0	41.0	78.0	95.0	95.0	78.0
70	44.0	57.0	58.0	46.0	84.0	104.0	104.0	87.0
80	45.0	58.0	60.0	48.0	87.0	107.0	108.0	90.0
90	44.0	57.0	58.0	46.0	85.0	107.0	106.0	87.0

B — $10^6 \times Y$ (λ = 0.1 m)

$10^6\ \bar{\epsilon}/\pi$ mrad	a mrad	b mm	L = 0.06 m, m^2 = 150	L = 0.06 m, m^2 = 0	L = 0.03 m, m^2 = 150	L = 0.03 m, m^2 = 0
5	25.0	0.2	35.0	36.0	38.0	40.0
5	50.0	0.1	36.0	41.0	46.0	53.0
5	80.0	0.0625	29.0	42.0	38.0	56.0
10	25.0	0.4	57.0	59.0	53.0	56.0
10	50.0	0.2	68.0	79.0	83.0	97.0
10	80.0	0.125	56.0	83.0	71.0	109.0

Legend

a angular acceptance
b spatial acceptance
$\bar{\epsilon}$ acceptance πab
L target length
m^2 angular dependence of production, production $\propto (1 - m^2\theta^2)$
λ absorbtion length (equal for p and $\bar{p}$)
Y relative yield. For $(d^2\bar{N}/dpd\Omega) = 0.13$ (GeV/c)$^{-1}$sr^{-1} per interaction for 80 GeV/c p and 5.4 GeV/c $\bar{p}$, tungsten target, and $\Delta p/p$ = 1%, $8(d^2\bar{N}/dpd\Omega)\Delta p = 0.056$.

of acceptance a, for several cases, and vs. the acceptance $\bar{\epsilon} = \pi$ ab, also for several cases. The constant of the angular dependence is quite arbitrarily chosen as m^2 = 150 rad^{-2}, i.e., the intensity is down by a factor of two at θ = 58 mrad. The table shows that even in the absence of multiple scattering optimum target length is considerably less than $\lambda/2$, especially for larger acceptances. As might be expected there is an optimum acceptance angle. For comparison we give in a few selected cases the yield factor for flat angular distribution (m^2 = 0).

D. We now consider the case where the line source is off-axis. Because an arbitrary displacement is hard to calculate we take the special case of translation in the x-direction by x_0. We obtain equations similar to those in paragraphs B and C with x replaced by $x-x_0$:

$$D = 2\, I_0[x'^2/a^2 + (x - x_0)^2/b^2] \cdot \quad (21)$$
$$\cdot [1 - m^2x'^2 - 1/3\ m^2x'^2\{x'^2/a^2 + (x - x_0)^2/b^2\}^{-1}.$$

D integrated over the common area for $x_0^2 \le b^2$ yields

$$\bar{N} = 8I_0ab\int_{\phi_1}^{\pi/2}[1-x_0^2b^{-2}\sin^2\phi]^{1/2} \cdot \\ \cdot [1-1/3m^2a^2\sin^2\phi\{2+3x_0^2b^{-2}-x_0^2b^{-2}\sin^2\phi\}]d\phi \quad (22)$$

where $\phi_1 = \pi/2 - \tan^{-1}(c/b)$.

The relative drop of the yield may be defined as

$$R = \bar{N}_{\text{off-axis}}/\bar{N}_{\text{on-axis}}. \quad (23)$$

In the case of $m^2a^2 \ll 1$, i.e., if the production is flat over $\phi \le a$, R is the ratio of the leading terms:

$$R = \int_{\phi_1}^{\pi/2} \frac{[1 - (x_0/b)^2\sin^2\phi]^{1/2}}{\pi/2 - \phi_1}\, d\phi. \quad (24)$$

This is tabulated for a few selected cases in Table IV. A proton beam of finite size can be

Table IV. Yield Ratios R for Off-Center Beam.

(m^2 = 150 rad^{-2}, L = 0.03 m)

$10^6\bar{\epsilon}/\pi$	a(mrad)	b(mm)	$10^6Y(x_0=0)$	$R(x_0=b/2)$	$R(x_0=b)$
5	50.0	0.1	46.0	0.93	0.60
10	50.0	0.2	83.0	0.92	0.56
20	50.0	0.4	132.0	0.91	0.49
20	80.0	0.25	128.0	0.92	0.58
40	50.0	0.8	177.0	0.89	0.37
40	80.0	0.5	203.0	0.91	0.53
40	100.0	0.4	157.0	0.92	0.56

Legend

x_0 displacement of line source transverse to z-axis. See Table III Legend for others.

considered as consisting of a bundle of line sources, each having the appropriate R, which can be averaged over the p-beam area to provide a proper definition of F_{geom}. Clearly a given proton beam radius is directly related to the spatial half-axis of the acceptance ellipse. From the table one sees that conservatively beam radius r should be $r < b/2$ and that $r = b$ is probably larger than optimum. The optimum can be determined only by consideration of the intensity distribution over the proton beam, the beam jitter, the multiple scattering and chromatic effects.

E. The yield we have calculated above will apply in practice only if the optimum matching is maintained for the entire momentum bite. We illustrate the variation of the matching for different momenta by considering the transformation of the acceptance ellipse from the collection lens focal point at the center of the target through the lens

of focal length f to an image plane a distance f downstream. Figure 5(a) shows the upright ellipse in the target focal plane which transforms to an upright ellipse [Fig. 5(b)] in the image plane for $\Delta p/p = 0$. The momentum dependence of the focal length can be written

$$\Delta f/f \approx (1/2 + kL \operatorname{cosec} 2kL)\ \Delta p/p, \quad (25)$$

where k is the focusing strength $\sqrt{B'/B\rho}$. In Fig. 5(c) we show the result of transforming the upright

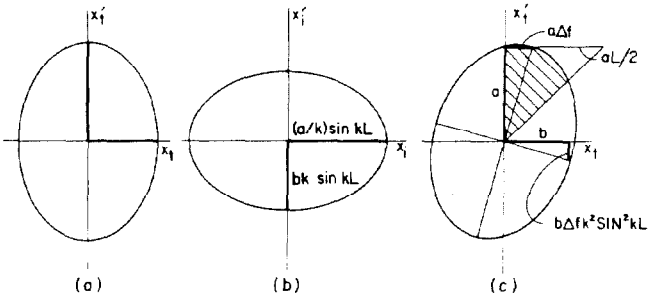

Fig. 5.

ellipse in the image plane back through the lens with its focal length being f + Δf. To first order in Δf the end of the angle semi-axis, which has coordinates $(x_t, x'_t) = (0, a)$ for $\Delta f = 0$, now lies at $(a\Delta f, a)$. Likewise the end of the aperture semi-axis now lies at $(b, -b\Delta f k^2 \sin^2 kL)$ instead of (b,0). By comparing Fig. 5(c) with Fig. 4, however, one can see that the overlap integral for the yield [Eq. (14)] is little affected by the tilt of the ellipse so long as $a\Delta f \ll b < aL/2$. For our application $a \sim 10^{-2}$, $b \sim 10^{-4}$, $f \sim 10^{-1}$, and $kL \sim 1$, so that $a\Delta f \approx 4 \cdot 10^{-5} \ll b \approx 2 \cdot 10^{-4} < aL/2 \approx 5 \cdot 10^{-4}$ for $\Delta p/p = 1\%$. If $a\Delta f = b$ is taken as a criterion for serious chromatic abberation one infers a momentum passband $\Delta p/p \approx 5\%$ for the collecting lens, a result which is confirmed by the monte carlo calculation described in the next section.

F. We evaluate the emittance of a point souce due to multiple coulomb scattering after a thickness h of scatterer; the contour on which the intensity is down by e^{-1} of the central intensity, i.e., the contour containing 84% of the scattered particles, has the form of a skew ellipse shown in Fig. 6 in the (x_s, x_s') plane at the end of the scatter. The coordinates of the marked points H and V on the tangent enclosing rectangle are

$$x_H = h\sqrt{\overline{x_s'^2}/2}, \qquad x'_H = \sqrt{2\,\overline{x_s'^2}}$$
$$x_V = h\sqrt{2\overline{x_s'^2}/3}, \qquad x'_V = \sqrt{3\overline{x_s'^2}/2}, \quad (26)$$

where the rms projected angle of multiple scattering is evaluated by the conventional expression

$$\overline{x_s'^2}^{1/2} \approx 0.014\ \text{GeV/c}\ \sqrt{h/X_0}/p\beta, \quad (27)$$

where X_0 is the radiation length and β is the velocity ratio v/c. The area of this ellipse is

$$E = \pi h\, \overline{x_s'^2}/\sqrt{3}, \quad (28)$$

which scales as h^2. By transforming this area to a convenient reference plane we can estimate the scattering effect by looking at the overlap of the scattering emittance with the acceptance; the pattern in the reference plane becomes a superposition of transformed ellipses each corresponding to a point in the plane for the case of no scattering. It depends on the particular phase point where the emittance lies when transformed back to, say, the mid-target plane. If the scattering contour falls partly outside the target emittance, the particles scattered out are not fully replaced by particles scattered in. We illustrate this point in Fig. 7

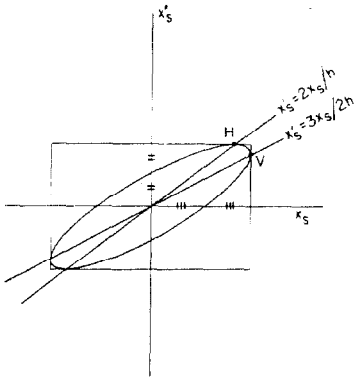

Fig. 6.

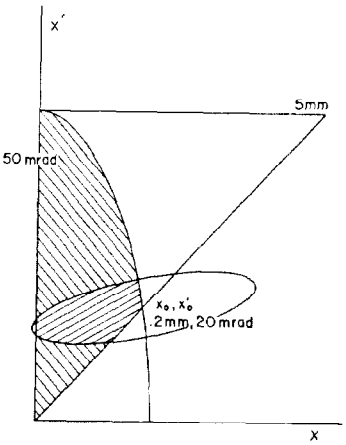

Fig. 7.

where we draw more-or-less to scale the 84% containment contour of a point on the intersection of the acceptance ellipse and the edge of the target emittance corresponding to a source at the upstream end of the target. The figure is drawn for a 2 cm tungsten target and an acceptance of $10\pi \times 10^{-6}$ m with semi-axes a = 50 mrad and b = 0.2 mm. The center of the scattering ellipse is at ~(0.2 mm, 20 mrad). The rms scattering angle is $\sqrt{\overline{x_s'^2}} \approx 4$ mrad and the scattering emittance $E_{84\%} = 0.185\pi \times 10^{-6}$ m lies ~50% outside the acceptance. Although this is a worst case example because the trajectory originates at the upstream end of the target, the sum of the loss over all trajectories is clearly significant and must be included in evaluating the relative merits of different target materials. When the acceptance ellipse is smaller the effect will clearly be of greater importance.

V. Monte Carlo Calculations

The most direct way to calculate the net effect of the simultaneous operation of all the processes discussed above is to follow the proton beam and the antiprotons it produces through the target and lithium lens in small steps. The sequence and location, as well as the type and strength, of the interactions occur randomly but under well known probabilities for each step. At each step a random choice is made among the possible processes of antiproton production, nuclear scattering, and multiple coulomb scattering according to the known distributions of interaction probability and angle.[6] In our calculation we do not include production by secondary interactions or energy loss by recoil or dE/dx by ionization. We do, however, include primary production in the lithium lens. We follow the evolution of x, x', y, y', and $\Delta p/p$ for both protons and antiprotons starting with 10^5 protons on target; all inelastic interactions are treated as antiproton production with the results normalized by the ratio of the $\bar{p}$ production cross section to the total cross section. The momentum value is not changed by the program but is used to determine the bending in magnetic field and the scattering.

After validating the program against easily calculable test cases, its results were compared with the analytic results above. When the input

conditions are sufficiently ideal to agree with the assumptions made in the analytic treatment the results are indeed reproduced. In particular we do find that with scattering eliminated the yield scales as $(\bar{\varepsilon}_x \cdot \bar{\varepsilon}_y)^{1/2}$. We also find that there is no significant variation of the acceptance of the lithium lens collector over a momentum band $\Delta p/p = 4\%$.

Because the monte carlo performs a five dimensional integration, however, questions regarding the effect of varying a particular parameter must be specified fully with respect to what coupled variation in other parameters is allowed to obtain optimum yield for the specified value of the parameter of interest. For example, if yield is to be evaluated as a function of acceptance, should the result be at optimum target length and proton beam width for each acceptance value or at some arbitrary fixed values? Fig. 8 shows yield plotted against acceptance ($\bar{\varepsilon} = \bar{\varepsilon}_x = \bar{\varepsilon}_y$) for the case when the beryllium

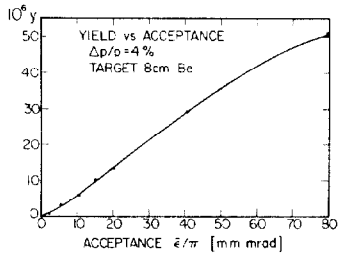

Fig. 8.

target length is optimum for $\bar{\varepsilon} = 15\pi \times 10^{-6}$ m. The importance of keeping target length matched as other parameters are varied is shown in Fig. 9 where yield

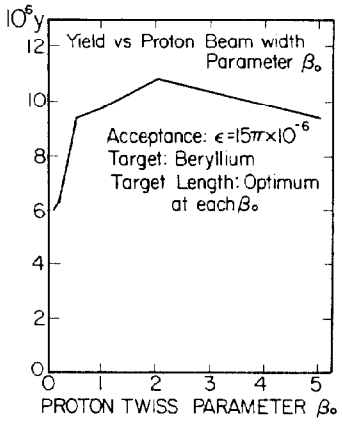

Fig. 9.

is plotted against the proton beam width Twiss parameter at the target focus, β_0. The smaller β_0, the larger the acceptance angle; however, the larger β_0, the longer the optimum target. We find that for **this target**, Be, at **this acceptance**, $15\pi \times 10^{-6}$ m, the optimum production occurs for $\beta_0 \approx 2$ m giving an rms beam spot $r_0 = \sqrt{\varepsilon\beta_0/\pi} \approx 0.32$ mm. For tungsten a smaller beam and shorter target is optimum.

The monte carlo calculation has not been pursued to construct comprehensive tables of yield vs. a reasonable range of all parameters. It has been used instead to check that the parameter dependences derived analytically remain valid for the more nearly realistic cases in which scattering, production in the collector, and production leaving the side of the target are considered. It has also been used to check cases in the neighborhood of a supposed optimum to make sure that it remains optimum when all parameters are considered. Finally it has been used to provide a reasonably good estimate for the absolute yield. We remark in this context that the yield for the currently accepted nominal targetting parameters ($\beta_0 = 1$ m, $\bar{\varepsilon} = 5\pi \times 10^{-6}$ m), which was estimated in Section III, is computed to be 0.8×10^{-6} m for both tungsten and beryllium targets by the monte carlo program; for this low acceptance case beryllium makes up for its lesser L_{eff}/λ by less scattering.

The above results may be optimum, however, only in a narrow sense because maximum $\bar{N}/N$ may not be the most economical when the entire cooling scheme is considered. For example, it was mentioned that a long Be target, while not as efficient, can produce a larger number of $\bar{p}$/spill. The present scheme calls for 2.6×10^{13} protons to produce 13 batches of 1.6×10^{6} $\bar{p}$ with momentum spread $\Delta p/p = 1\%$. After stacking and fast cooling of the $\bar{p}$ batches in the precooler one has 2.1×10^{7} $\bar{p}$ with a momentum spread of 2%. The monte carlo result shows that 1.4×10^{7} can be obtained by coalescing 2.7×10^{13} protons into 1/13 of the Main Ring[7] and collecting the antiprotons from a single fast spill on a 26 cm beryllium target with 2% momentum bite. The proton intensity cited in the comparison is based on applying the necessary beam preparation for each approach to current Main Ring operational intensity. These two approaches are close enough so that secondary considerations like relative simplicity or reliability could outweigh the difference in yield. Optimization decisions of this broader type are still being discussed for the Fermilab antiproton source, but the basic precooler described in the Tevatron Phase I Design Report[1] seems adaptable to a wide range of variations on the basic production, cooling, accumulation scheme.

References

1. **Design Report Tevatron Phase I Project**, Fermi National Accelerator Laboratory (1980).
2. J. MacLachlan et al., "Pulsed High Current Optics in $\bar{p}$ Production at 5.4 GeV/c," to be published in IEEE Trans. Nucl. Sci.
3. J. W. Cronin in **1977 Summer Study**, (J. K. Walker, ed.) V. 1, 269, Fermilab (1977).
4. Proc. of the Workshop on Producing High Luminosity High Energy Proton-Antiproton Collisions, March 21-31, 1978, Lawrence Berkeley Laboratory Report LBL-7574 UC-34c Conf-780345 (1978)
5. A. VanGinneken, Fermilab FN-272 (1975).
6. J. MacLachlan et al., Fermilab TM-244 (May 1970).
7. J. Griffin et al., IEEE Trans. Nucl. Sci. **NS-26**, No. 3, 3589 (1979). Refinements to the bunch compression scheme to handle 12 batches have been worked out, J. Griffin (private communication).